

## Accepted Manuscript

Title: Direct activation of CH<sub>4</sub> to oxygenates and unsaturated hydrocarbons using N<sub>2</sub>O on Fe-modified zeolites

Author: Kyung Soo Park Jeong Hwa Kim So Hyun Park  
Dong Ju Moon Hyun-Seog Roh Chan-Hwa Chung Soong Ho  
Um Joon-Hwan Choi Jong Wook Bae



PII: S1381-1169(16)30482-4  
DOI: <http://dx.doi.org/doi:10.1016/j.molcata.2016.11.008>  
Reference: MOLCAA 10105

To appear in: *Journal of Molecular Catalysis A: Chemical*

Received date: 30-7-2016  
Revised date: 29-10-2016  
Accepted date: 5-11-2016

Please cite this article as: Kyung Soo Park, Jeong Hwa Kim, So Hyun Park, Dong Ju Moon, Hyun-Seog Roh, Chan-Hwa Chung, Soong Ho Um, Joon-Hwan Choi, Jong Wook Bae, Direct activation of CH<sub>4</sub> to oxygenates and unsaturated hydrocarbons using N<sub>2</sub>O on Fe-modified zeolites, *Journal of Molecular Catalysis A: Chemical* <http://dx.doi.org/10.1016/j.molcata.2016.11.008>

This is a PDF file of an unedited manuscript that has been accepted for publication. As a service to our customers we are providing this early version of the manuscript. The manuscript will undergo copyediting, typesetting, and review of the resulting proof before it is published in its final form. Please note that during the production process errors may be discovered which could affect the content, and all legal disclaimers that apply to the journal pertain.

Submitted to the *Journal of Molecular Catalysis A: Chemical*

**Direct activation of CH<sub>4</sub> to oxygenates and unsaturated hydrocarbons using N<sub>2</sub>O on Fe-modified zeolites**

Kyung Soo Park<sup>1</sup>, Jeong Hwa Kim<sup>1</sup>, So Hyun Park<sup>1</sup>, Dong Ju Moon<sup>2</sup>, Hyun-Seog Roh<sup>3</sup>,  
Chan-Hwa Chung<sup>1</sup>, Soong Ho Um<sup>1</sup>, Joon-Hwan Choi<sup>4</sup>, Jong Wook Bae<sup>1,\*</sup>

<sup>1</sup>School of Chemical Engineering, Sungkyunkwan University (SKKU), Suwon, Gyeonggi-do, 440-746, Republic of Korea

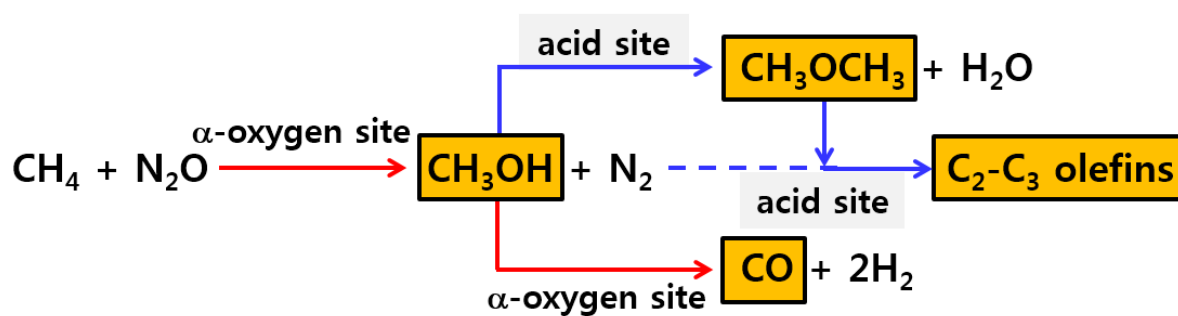
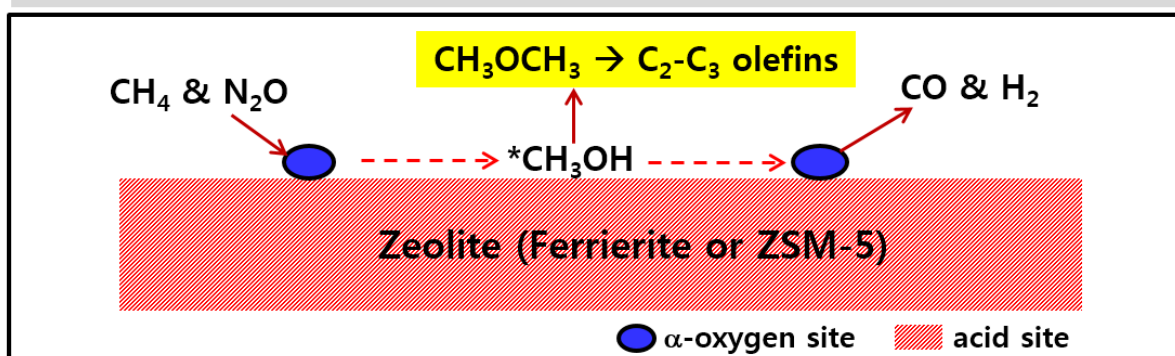
<sup>2</sup>Clean Energy Research Center, Korea Institute of Science and Technology (KIST), 136-791 Seoul, Republic of Korea

<sup>3</sup>Department of Environmental Engineering, Yonsei University, 1 Yonseidae-gil, Wonju, Gangwon 220-710, Republic of Korea

<sup>4</sup>Functional Ceramics Department, Korea Institute of Materials Science (KIMS), Changwon, Gyeongnam 642-831, Republic of Korea

\*Corresponding author (J.W. Bae): Tel.: +82-31-290-7347; Fax: +82-31-290-7272; E-mail address: finejw@skku.edu

## Graphical abstract

Direct activation of  $\text{CH}_4$  to oxygenates using  $\text{N}_2\text{O}$  on Fe-modified zeolites

## HIGHLIGHTS

- Direct activation of  $\text{CH}_4/\text{N}_2\text{O}$  to oxygenates was investigated on the Fe-modified zeolites.
- Amount of  $\alpha$ -oxygen and Bronsted acid sites significantly changed the product distribution.
- Fe/FER showed a high activity due to a larger amount of  $\alpha$ -oxygen and acidic sites.

**ABSTRACT**

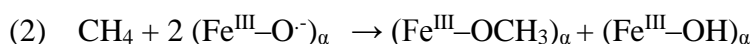
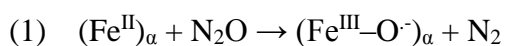
Direct activation of CH<sub>4</sub> to oxygenates and unsaturated light hydrocarbons was investigated using Fe-modified ZSM-5 and Ferrierite (FER) for a partial oxidation of CH<sub>4</sub> with N<sub>2</sub>O oxidant. The amount of active  $\alpha$ -oxygen sites and number of Bronsted acid sites on the Fe-modified zeolites were well correlated with CH<sub>4</sub> conversion rate and product distributions. The amount of  $\alpha$ -oxygen sites was largely changed according to preparation method such as wet impregnation or ion-exchange of iron precursor and types of zeolites. A large number of Bronsted acid sites and  $\alpha$ -oxygen sites on the Fe-modified FER revealed a higher oxygenate formation such as methanol and dimethyl ether (DME) with CO<sub>x</sub>, and a larger number of strong acid sites on Fe-modified ZSM-5 was also responsible for a higher selectivity to light hydrocarbons by a successive dehydration of oxygenates formed. The different catalytic performances were verified through proper measurements of the amount and type of acidic sites as well as the  $\alpha$ -oxygen sites measured by N<sub>2</sub>O pulse chemisorption. The Fe-modified FER prepared by impregnation method possessed a larger amount of  $\alpha$ -oxygen sites due to abundant Bronsted acid sites, which was responsible for a higher rate of CH<sub>4</sub> conversion to oxygenates with the help of N<sub>2</sub>O decomposition on the  $\alpha$ -oxygen sites originated from iron oxide nanoparticles.

**Key words:** CH<sub>4</sub> activation; N<sub>2</sub>O oxidant; Fe-modified zeolites; Acid sites;  $\alpha$ -oxygen sites.

## 1. Introduction

A direct utilization of CH<sub>4</sub>, which is a main component of natural gas (or shale gas) and one of important greenhouse gases (GHG), to useful chemicals or fuels has been widely studied due to an increased demand of clean fuels from alternative resources [1] and to reduce the emission of GHG. Compared to an indirect conversion of natural gas to useful chemicals through various syngas production processes, a partial oxidation of CH<sub>4</sub> with oxidants such as oxygen or N<sub>2</sub>O to oxygenates as basic petrochemical feedstocks like methanol, formaldehyde, dimethyl ether (DME) or formic acid seems to be one of the most attractive methods due to its simple process scheme for direct conversion of CH<sub>4</sub> [2-3]. Among those oxygenates, DME was considered as one of clean fuels owing to its lower emission of air-pollutants by producing 31,350 kJ/kg of heat [4], which also has similar physical properties with liquefied petroleum gas (LPG). However, some drawbacks of a direct partial oxidation of CH<sub>4</sub> to oxygenates should be previously solved for commercial application by efficiently prohibiting thermodynamically favorable and competitive combustion reaction by consecutive reaction of formed oxygenated intermediates to fully combusted unuseful CO<sub>x</sub> (CO and CO<sub>2</sub>). To solve these shortcomings, many catalytic systems for direct methane activations have been tested by using the active molybdate, vanadate or iron phosphate species supported on the (meso)porous silica, which was applied for the production of formaldehyde mainly [5-7]. In addition, some transition metal oxides or metal loaded zeolites have been also extensively investigated due to their bifunctional activity of metallo-zeolite, which have not only solid acid functionalities of the zeolite but also active sites for the activation of thermodynamically stable light hydrocarbons to oxygenates or aromatic components [8-15]. Recently, substantial attentions have been paid to develop proper catalytic systems by using transition metals such as Fe, Co or Cu incorporated on the solid-acid ZSM-5 since these catalysts showed a superior activity for a direct oxidation of CH<sub>4</sub> to oxygenates even at a relatively low temperature with

the help of soft oxidants such as  $\text{N}_2\text{O}$  and  $\text{H}_2\text{O}_2$  [16-20]. Among them, Fe-ZSM-5 has been widely investigated due to its higher activity for selective catalytic reduction (SCR) of  $\text{N}_2\text{O}$  pollutant with ammonia or light paraffins, which was known as one of the important greenhouse gases emitted from automobiles [21-23]. In general, iron-incorporated zeolites have been generally reported to have active sites for a selective  $\text{N}_2\text{O}$  decomposition. Although the structures of the active iron sites named as  $\alpha$ -sites are still on debate, it has been known to be formed as the reduced form after high temperature treatment [24]. While decomposing  $\text{N}_2\text{O}$  molecules on the active  $\alpha$ -sites, two of iron species seem to be bridged with adjacent oxygen atom originated from  $\text{N}_2\text{O}$  to form Fe-O-Fe diiron complex (known as  $\alpha$ -oxygen sites) through equation (1). These  $\alpha$ -oxygen sites are also known to have reactive natures which are capable to oxidize the stable hydrocarbons such as methane and benzene to methanol and phenol respectively with reversible redox properties by the following equation (2) [25-27]. Based on the mechanisms, an activation of  $\text{CH}_4$  molecules on  $\alpha$ -oxygen sites ( $\text{O}_\alpha$ ) can proceed by a hydrogen abstraction mechanism with high reaction rate even at an ambient temperature. The fragments formed by an activated  $\text{CH}_4$  have been reported to form methoxy and hydroxyl groups while reacting with  $\alpha$ -oxygen sites with a stoichiometric ratio of  $\text{CH}_4:\text{O}_\alpha = 1:2$  by the equation (2) [28]. A rate determining step has been known to be desorption step of products [19,28], and an amount of active  $\alpha$ -oxygen sites originated from Fe-O-Fe diiron complexes has been also closely related with the amount of surface Bronsted acid sites on the solid-acid zeolites as well [24,29,30].



In the present study, a direct synthesis of useful oxygenates such as methanol and DME as

well as C<sub>2</sub> – C<sub>3</sub> light hydrocarbons through an oxidative dehydrogenation of CH<sub>4</sub> using N<sub>2</sub>O oxidant was reported using Fe-modified zeolites to verify the roles of  $\alpha$ -oxygen sites as well as Bronsted acid sites, where the hybrid Fe-ferrierite catalytic systems have been scarcely investigated in terms of product distributions as far as we know. The pristine ZSM-5 and ferrierite (FER) zeolites were modified using iron precursor through two different preparation methods such as a simple wet impregnation and ion-exchange in an aqueous solution to elucidate the roles of amount of surface  $\alpha$ -oxygen sites as well as Bronsted acid sites. The number of surface Bronsted acid sites and amount of active  $\alpha$ -oxygen sites on Fe-modified zeolites simultaneously altered CH<sub>4</sub> conversion rate and product distribution of oxygenates and light hydrocarbons.

## 2. Experimental

### 2.1. Catalyst preparations and activity measurements

A solid acid zeolite of NH<sub>4</sub>-form FER was purchased from Zeolyst (Si/Al ratio of 9, CP-914C), and H-form ZSM-5 was provided from Zeocat (Si/Al ratio of 28, PZ-50H). NH<sub>4</sub>-form FER was previously calcined at 500 °C for 3 h under air atmosphere to make H-form FER. To prepare Fe-modified zeolites (Fe/zeolites) such as the Fe/ZSM-5 and Fe/FER, the powder-type zeolite was previously dispersed in deionized water, and a desired amount of iron precursor of Fe(NO<sub>3</sub>)<sub>3</sub>•9H<sub>2</sub>O (Samchun, 98.5% purity) was added in the slurry at a fixed 7wt%Fe based on total weight of zeolite. After thoroughly mixing the above slurry in a rotary evaporator for 1 h, vacuum evaporation was carried out at 60 °C to prepare impregnated Fe/zeolites. After drying overnight at 110 °C, the sample was calcined at 550 °C for 6 h under air atmosphere with a heating rate of 1 °C/min. As-prepared catalysts are denoted as Fe/ZSM-5(IMP) and Fe/FER(IMP), respectively. In addition, a liquid phase ion-exchange of the iron precursor on H-form ZSM-5 and FER was also applied to prepare Fe-modified zeolites with a

fixed amount of  $\text{Fe}(\text{NO}_3)_3 \cdot 9\text{H}_2\text{O}$  precursor in an aqueous solution by vigorously stirring at 80 °C for 24 h. After washing and filtering, the sample was further dried at 110 °C in an oven overnight followed by calcining at 550 °C for 6 h in air environment with a heating rate of 1 °C/min. After the calcination, the powder was crushed in the particle size less than  $\sim 100 \mu\text{m}$  to avoid an internal diffusion limitation on general heterogeneous catalysts [31-32]. The as-prepared Fe/zeolites are denoted as the Fe/ZSM-5(IE) and Fe/FER(IE).

Catalytic activity for a direct  $\text{CH}_4$  oxidation to oxygenates and hydrocarbons was evaluated in a fixed-bed tubular reactor with an outer diameter of 9 mm. Prior to activity test, 0.1 g of Fe/zeolite was loaded in the reactor, and reduced under a flow of 5vol%  $\text{H}_2$  balanced with  $\text{N}_2$  at 700 °C for 3 h. After the reduction, the temperature was cooled down to room temperature, and reactants with a molar ratio of  $\text{CH}_4/\text{N}_2\text{O} = 2.5$  were fed into the reactor with an internal standard gas of 5vol% He. The reaction was carried out at  $T = 280 \text{ °C}$ ,  $P = 0.1 \text{ MPa}$ , and space velocity ( $\text{SV} = 12000 \text{ L}(\text{total gas})/(\text{kg}_{\text{cat}} \cdot \text{h})$ ) for 10 h, and the catalytic activity at steady-state after 5 h on stream was compared using an average values. Additional activity test for a methanol conversion to oxygenates and hydrocarbons was further carried out in a same fixed-bed tubular reactor with 0.1 g catalyst to verify activity and product distribution of the conversion of methanol intermediates formed by direct  $\text{CH}_4$  activation from  $\text{CH}_4/\text{N}_2\text{O}$ . Prior to the activity test, the as-prepared catalyst was reduced at 700 °C for 3 h under a flow of 5vol%  $\text{H}_2/\text{N}_2$ . Catalytic activity for methanol conversion was measured for 5 h using the reactant of 10vol%  $\text{N}_2\text{O}/\text{He}$  gas at a liquid methanol feed rate of 0.013 mL/min at the reaction conditions of  $T = 290 \text{ °C}$ ,  $P = 0.1 \text{ MPa}$ , and  $\text{SV} = 12000 \text{ L}/(\text{kg}_{\text{cat}} \cdot \text{h})$ . The effluent gases from the reactor were measured continuously by using a gas chromatograph (YL6500, Younglin). Using a thermal conductivity detector (TCD) connected with a Carboxen 1000 packed column,  $\text{CH}_4$ ,  $\text{N}_2$ ,  $\text{H}_2$ ,  $\text{CO}_x$ , and  $\text{N}_2\text{O}$  were analyzed. The formed hydrocarbons and all oxygenates by direct  $\text{CH}_4$  activation were also analyzed by using a flame ionization detector

(FID) connected with a HP PLOT Q capillary column. The rate of N<sub>2</sub>O conversion was calculated using the variation of reactant concentration based on an internal standard gas of He, and the rate of CH<sub>4</sub> conversion and product distributions at steady-state for last 5 h on stream was calculated based on total carbon balance.

## 2.2. Catalyst characterization

Powder X-ray diffraction (XRD) analysis of the fresh and used Fe/zeolites was performed to verify the crystalline phases and variations of crystallinity before and after reaction using X'Pert<sup>3</sup> Powder (PANalytical) operated at 40 kV and 100 mA with Cu-K $\alpha$  radiation of 0.15406 nm in the range of 5 - 35° at a scanning rate of 4°/min. The elemental composition of Fe and Si/Al molar ratio on the fresh Fe/zeolites were also determined by X-ray fluorescence (XRF) analysis using Bruker S4 operated at 60 kV and 150 mA. The surface morphology and variation of crystallite sizes of iron oxides on the fresh and used Fe/FER(IMP) and Fe/FER(IE) were further characterized using transmission electron microscopy (TEM) with a TECNAI G2 instrument operated at an accelerating voltage of 200 kV.

Temperature programmed reduction with hydrogen (H<sub>2</sub>-TPR) was carried out using BELCAT-M instrument to characterize reduction behaviors of the Fe/zeolites. For the TPR analysis, 10vol%H<sub>2</sub> balanced with Ar was used with 30 mg fresh sample which was previously treated with He at a flow rate of 30 mL/min at 500 °C for 1 h to remove any contaminants and adsorbed water. After the pretreatment, the temperature was cooled down to 100 °C and kept for 0.5 h, and the temperature was subsequently increased up to 800 °C with a ramping rate of 10 °C/min. The effluent gases were passed through a molecular sieve to remove water formed during TPR analysis and the amount of hydrogen consumption was recorded using TCD. Temperature programmed desorption of ammonia (NH<sub>3</sub>-TPD) was carried out using the same BELCAT-M instrument to characterize the amount of acid sites on

the fresh Fe/zeolites. Before the NH<sub>3</sub>-TPD analysis, the sample was heated up to 250 °C with a ramping rate of 10 °C/min and maintained at the same temperature for 2 h to eliminate any contaminants and water adsorbed on the catalyst surfaces. After the pretreatment, the sample was cooled down to 100 °C, and NH<sub>3</sub> gas with a purity of 99.999% was introduced on the sample for 1 h at a flow rate of 50 mL/min followed by purging for 1.5 h to remove physisorbed NH<sub>3</sub> molecules. The sample was analyzed by heating from 100 to around 600 °C at a ramping rate of 10 °C/min, and the amount of desorbed NH<sub>3</sub> was analyzed by using TCD.

To compare relative amount of Bronsted and Lewis acid sites on the Fe/zeolites, Fourier-transform infrared (FT-IR) spectroscopy analysis of an adsorbed pyridine (Py-IR) was carried out using FT-IR spectrometer of Nicolet 6700 (Thermo fisher scientific). For the Py-IR analysis, 30 mg of fresh sample was previously pelletized to a self-supported thin pellet, and the temperature of FT-IR cell was raised up to 150 °C in a vacuum atmosphere at a ramping rate of 15 °C/min to remove the adsorbed water and any contaminants. After the cell temperature was stabilized at 150 °C, FT-IR background spectrum of the sample was taken at a scanning speed of 32 scans/s with a resolution of 4 cm<sup>-1</sup>. After the collection of background spectrum, 3 μL of pyridine was injected into the static vacuum system by using microsyringe for the adsorption of pyridine to the pretreated sample pellet for 15 min. The physisorbed and residual pyridine molecules was evacuated at 150 °C for 0.5 h, and the Py-IR spectra of the chemisorbed pyridine molecules were obtained on the fresh Fe/zeolites.

N<sub>2</sub>O titration was further carried out to measure the amount of active  $\alpha$ -oxygen sites (O <sub>$\alpha$</sub> ) using AutoChem II 2920 instrument (Micrometrics). For the N<sub>2</sub>O titration analysis, 100 mg sample was previously reduced at 700 °C for 3 h under 10vol%H<sub>2</sub> balanced with Ar, and cooled down to 280 °C. The pulses of 10 vol%N<sub>2</sub>O balanced with He were continuously introduced up to a full saturation of active  $\alpha$ -oxygen sites on the Fe/zeolites. The consumed amount of N<sub>2</sub>O was calculated from the measured amount of the formed N<sub>2</sub> using TCD.

Finally, the amount of the  $\alpha$ -oxygen sites on the reduced Fe/zeolites was evaluated from the accumulated amount of  $N_2O$  consumption using a stoichiometry of  $N_2O/O_\alpha = 1.0$ .

Temperature programmed surface reaction (TPSR) of the used Fe/zeolites was carried out to verify the amount of deposited coke precursors by using a BELCAT-M connected with gas chromatography-mass spectrometer (GC-MS) (YL6900 GC/MSD, Younglin) equipped with a deactivated fused silica capillary blank column. A 30mg of the used sample was loaded and subsequently pretreated with 30 mL/min of He at 500 °C for 1 h. After the pretreatment, the sample was cooled down to 50 °C and 10vol%  $H_2$  balanced with Ar was introduced by increasing temperature up to 700 °C with a ramping rate of 15 °C/min for the complete hydrogenation of the formed coke precursors to  $CH_4$ . The effluent gases were passed through molecular sieve for eliminating the formed  $H_2O$ . The MS signals were collected in range of  $amu = 2-50$  per second, and the selected  $m/z$  values assigned to methane fragments ( $m/z = 14$  and 15) was collected to exclude the MS signals from  $H_2O$  fragments.

### 3. Results and Discussion

#### 3.1. Physicochemical properties of the Fe-modified zeolites

The elemental compositions of the fresh Fe/zeolites measured by XRF are summarized in **Table 1**. The Fe/zeolites prepared by impregnation method showed similar iron contents with the values of 7.3 and 7.8wt% on the fresh Fe/FER(IMP) and Fe/ZSM-5(IMP), respectively. However, since a larger amount of acid sites exists on the FER due to a lower Si/Al ratio of 9 than that of ZSM-5 of 28, the composition of iron species was found to be slightly higher on the ion-exchanged Fe/FER than that of Fe/ZSM-5 with an iron content of 6.4wt% on the Fe/FER(IE) and that of 4.8wt% on the Fe/ZSM-5(IE). The Si/Al ratio after Fe modification of the zeolites was also found to be similar to parent zeolites in both FER and ZSM-5. With the help of  $NH_3$ -TPD and TEM analyses in following section, the dispersion of iron species on

the Fe/zeolites seems to be higher on the ion-exchanged Fe/ZSM-5(IE) and Fe/FER(IE) than other Fe/zeolites, which was attributed to the adsorption character of iron precursor on the Bronsted acid sites selectively, especially on the Fe/FER(IE) having a larger amount of Bronsted acid sites as summarized in **Table 1**.

XRD patterns of the Fe/zeolites before and after reaction are displayed in **Figure 1** and the characteristic diffraction peaks of bare ZSM-5 and FER are also displayed in supplementary **Figure S1** which showed similar diffraction patterns with previously reported ones [33-35]. The each crystalline structure of the zeolites was preserved even after Fe modification and reaction at 280 °C for 10 h. However, the characteristic diffraction peaks of iron species were not clearly observed due to its higher dispersion on the ZSM-5 and FER possibly. In addition, the XRD peak intensities of the characteristic diffraction peaks on the bare zeolites were decreased after Fe modification, especially on the Fe/ZSM-5(IMP) and Fe/FER(IMP), due to a larger amount of iron concentration as shown in **Figure 1(a)**. Interestingly, the characteristic diffraction peaks of the bare ZSM-5 and FER on the used Fe/zeolites were preserved with relatively lower peak intensity as shown in **Figure 1(b)**. This observation suggests a possible structural deformation on the Fe/zeolites coming from a high temperature reduction at 700 °C or deposition of coke precursors during the reaction. These significant decreases of the characteristic peak intensities of the FER and ZSM-5 can be also attributed to a slight dissolution of aluminosilicate crystals in an acid iron nitrate precursor solution as well [36]. In addition, the relative crystallinity of the fresh and used Fe/zeolites was further calculated by comparing integrated peak areas of the characteristic diffraction peaks in the range of 6 - 10° for the Fe/ZSM-5 and 8 - 10° for the Fe/FER. The variations of the crystallinity of the Fe/zeolites also revealed a large deformation of the crystallinity of zeolites after reaction. As summarized in **Table 1**, the decreased crystallinity of the Fe/zeolites before and after reaction was found to be more significant on the Fe/ZSM-5 by showing the relative

crystallinity from 35 to 15 on the Fe/ZSM-5(IMP), 36 to 18 on the Fe/ZSM-5(IE) than those of the Fe/FER from 44 to 30 on the Fe/FER(IMP) and 72 to 37 on the Fe/FER(IE), respectively. A large decrease of crystallinity on the Fe/ZSM-5 during the reaction can be attributed to the preferentially deposition of iron nanoparticles on the outer surfaces of the ZSM-5 due to a smaller amount of acid sites than the FER, which also caused the structural deformation of zeolites. The variation of relative crystallinity of the Fe/zeolites after reaction was found to be in the orders of Fe/FER(IMP) < Fe/FER(IE) < Fe/ZSM-5(IE) < Fe/ZSM-5(IMP) with the respective values of 31.8, 48.6, 50, and 57.1, which suggests the significant structural collapses of the Fe/zeolites after reaction especially on the Fe/ZSM-5 and the trends are related with the coke deposition as discussed in the following TPSR results.

Since the present ZSM-5 having a higher Si/Al ratio than that of FER possesses a smaller amount of acid sites with a lower ion-exchange capacity, an excess amount of iron species can be preferentially deposited on the outer surfaces of the ZSM-5 in a form of iron oxide nanoparticles [37,38]. These phenomena can be also responsible for a decreased catalytic stability of the zeolite structures under the reaction condition due to a less possibility of metal incorporation in the frameworks of zeolites [39], especially on the Fe/ZSM-5. The relative crystallinity observed on the used Fe/ZSM-5(IMP) and Fe/ZSM-5(IE) with the respective values of 15 and 18 was more significant than those of the used Fe/FER with the respective values of 30 and 37 on the used Fe/FER(IMP) and Fe/FER(IE). Therefore, the Fe/ZSM-5 and Fe/FER prepared by ion-exchange method showed a lower content of iron species than those of the impregnation method because the iron precursor can be heterogeneously deposited on the zeolite surfaces through an impregnation method. The Fe/ZSM-5(IE) revealed a less amount of Fe loading compared to the Fe/FER(IE) due to a lack of ion exchanging capacity with the protons attached on the Bronsted acid sites of ZSM-5 compared to FER. Therefore, the deposited iron species seems to exist in cationic forms of iron species on the acid sites of

zeolites with a partial formation of crystalline iron oxide nanoparticles on the outer surface of zeolites, and the size of iron nanoparticles seems to be much smaller on the Fe/zeolites prepared by ion-exchange method which can be hardly detected by XRD analysis due to its small particle size or overlapping with zeolite structures.

To verify the reduction behaviors of the Fe/zeolites, H<sub>2</sub>-TPR analysis was performed and the reduction patterns are displayed in **Figure 2**. Hydrogen was consumed from 200 °C and the distinctive reduction peaks of iron oxides were observed at around 290 and 450 °C with a small peak at around 650 °C. All reduction patterns of the Fe/zeolites revealed the presence of different iron species on the surfaces through different interactions. Since iron (III) nitrate precursor was used for the modification of zeolites having the character of facile formation of Fe<sup>3+</sup> cations after decomposition, the Fe<sup>3+</sup> species can exist in a cationic form or Fe<sup>3+</sup>-OH and stabilized Fe<sup>2+</sup> species on the acid sites [40]. Moreover, an ion-exchanged cationic iron species can be easily aggregated on the acid sites to form iron oxide nanoparticles during a calcination step as well [41]. Therefore, various states of iron species such as isolated Fe cationic monomers, dimers, oligomers as iron oxo species or iron oxide nanoparticles can be possibly formed due to an excess usage of iron precursor above an ion-exchange capacity of the ZSM-5 or FER zeolites, which were responsible for the observation of multiple reduction peaks on the Fe/zeolites [41-44]. As shown in **Figure 2**, all Fe/zeolites showed a shoulder reduction peak in the range of 200 - 300 °C which was attributed to the reduction of the cationic iron species [40]. The larger peak intensity below 300 °C on the Fe/FER compared to the Fe/ZSM-5 was attributed to a larger ion exchange capacity on the Fe/FER having a larger amount of acid sites, especially on the Fe/FER(IMP). In addition, the Fe/ZSM-5 showed a smaller intensity of reduction peaks than those of the Fe/FER and the distinguishable peaks at around 400 - 600 °C can be attributed to the reduction of iron oxide nanoparticles formed on the outer surfaces of zeolites [39,45], especially large on the Fe/FER(IMP) and lower

reduction temperature on the Fe/FER(IE). Therefore, the Fe/FER(IMP) showing larger reduction peak intensity compared to the Fe/ZSM-5 revealed the well dispersion of iron nanoparticles on the abundant acid sites of FER with a relatively stronger interaction than Fe/FER(IE). The Fe/FER(IMP) was preferentially reduced in a wide range of temperatures than the Fe/ZSM-5 without showing a higher reduction peak above 650 °C, and it also leads to a possible formation of homogeneously distributed iron oxide nanoparticles. In terms of the formation of  $\alpha$ -oxygen sites on the Fe/zeolites, the ion-exchanged  $\text{Fe}^{3+}$  species adsorbed on the Bronsted acid site selectively [40] and the aggregated iron oxide nanoparticles can suppress amounts of active  $\alpha$ -oxygen sites, which seems to be dominant on the Fe/FER(IMP). Based on the results of TPR and surface acidity measurements, the ion-exchanged cationic iron species on the Bronsted acid sites and abundant formation of well-dispersed iron oxide nanoparticles were responsible for a preferential formation of active  $\alpha$ -oxygen sites as well, which are in line with the results of  $\text{N}_2\text{O}$  titration and  $\text{NH}_3$ -TPD in the following section.

### 3.2. Catalytic activities on the Fe-modified zeolites

The rates of  $\text{CH}_4$  and  $\text{N}_2\text{O}$  conversion with product distribution at steady-state using average values are summarized in **Table 2** and **Figure 3**. Although conversion of  $\text{CH}_4$  was observed below 1% with a maximum conversion on the Fe/FER(IMP) due to a difficult activation of  $\text{CH}_4$  in our reaction conditions, all Fe/zeolites revealed significantly different product distributions. Catalytic activity in a gas-phase on the Fe/FER was found to be higher than that of the Fe/ZSM-5 irrespective to the preparation methods. The rate of  $\text{CH}_4$  conversion was found to be 3.11 and 2.42  $\text{mmol}/(\text{g}_{\text{cat}}\cdot\text{h})$  on the Fe/FER(IMP) than Fe/FER(IE), respectively. The highest rate of  $\text{N}_2\text{O}$  conversion was also observed on the Fe/FER(IMP) with a value of 5.40  $\text{mmol}/(\text{g}_{\text{cat}}\cdot\text{h})$ , and the variations of the rates of  $\text{CH}_4$  and  $\text{N}_2\text{O}$  conversion as shown in **Figure 3** were not significant during 10 h on stream on all Fe/zeolites catalysts which also

supports the insignificant deactivation of the catalysts. However, the significant changes of product distributions were observed by showing a higher selectivity to oxygenates (mainly methanol and DME with insignificant byproducts) and CO<sub>x</sub> on the Fe/FER and by revealing a higher selectivity to unsaturated C<sub>2</sub>-C<sub>3</sub> hydrocarbons and oxygenates on the Fe/ZSM-5. For example, the selectivity of CO with a value of 48.9% and that of oxygenates with 47.6% (DME selectivity of 27.9%) were observed on the Fe/FER(IMP) and the similar values were observed on Fe/FER(IE). However, a higher selectivity to light olefinic hydrocarbons such as ethylene and propylene on the Fe/ZSM-5 was observed on the Fe/ZSM-5(IMP) with the value of 42.2% and a large amount of oxygenates of 57.8% (DME selectivity of 37.6%) was also observed instead of oxidized CO<sub>x</sub> products with the similar values on the Fe/ZSM-5(IE). Small amount of hydrogen was also produced from this reaction, and H<sub>2</sub>/CO ratio was found to be around 0.20, which is far from a theoretical value of 2 for the possible methanol steam reforming due to a small amount of H<sub>2</sub>O formed on the Fe/FER(IMP). Based on the observed lower H<sub>2</sub>/CO ratio on the most active Fe/FER(IMP), CO was not mainly formed from the steam reforming of methanol product and it seems to be originated from a direct combustion of methane possibly with the help of active  $\alpha$ -oxygen species. As shown in **Figure 3**, all of the catalysts were deactivated slowly during the reaction of 10 h with increasing the selectivity to oxygenates and decreasing hydrocarbons and CO<sub>x</sub> products due to the possible aggregation of iron nanoparticles during the reaction.

In addition, the catalytic activity changes of the Fe/FER(IMP) at different space velocities are summarized in **Table S1** and **Figure S2** with time on stream. By increasing space velocities from 6000 to 18000 L/(kg<sub>cat</sub>·h), the rate of CH<sub>4</sub> and N<sub>2</sub>O conversions were decreased from 6.23 to 2.27 mmol/(g<sub>cat</sub>·h) and from 10.42 to 4.20 mmol/(g<sub>cat</sub>·h) due to a short residence time in a catalyst-bed. However, the oxygenates including DME and methanol were gradually increased from 22.7 to 50.5% with an increase of space velocity by simultaneously

decreasing the selectivity to hydrocarbons and combusted CO<sub>x</sub> products due to a facile oxidation of intermediates at a longer residence time selectively on the active  $\alpha$ -oxygen sites.

The effects of reaction temperatures to catalytic activity were also investigated on the Fe/FeO(IMP) at different temperatures from 240 to 360 °C and the results are summarized in **Table S2** and **Figure S3** with time on stream (h). As the temperatures were increased, the rate of conversions of CH<sub>4</sub> and N<sub>2</sub>O were dramatically increased from 0.18 to 48.20 mmol/(g<sub>cat</sub>·h) and from 1.22 to 145.38 mmol/(g<sub>cat</sub>·h), respectively. The combustion reaction of CH<sub>4</sub> to form CO<sub>x</sub> products was preferential at high temperature above 300 °C. At a lower temperature of 240 °C, even though the amount of reacted methane was quiet around 0.18 mmol/(g<sub>cat</sub>·h), the oxygenates including DME and methanol (95.7%) and hydrocarbons (4.3%) were mainly formed without CO<sub>x</sub> formation. Above the temperature of 260 °C, CO was formed with the selectivity of 55.0% based on total carbons and the selectivity to oxygenates was dramatically decreased to 42.4%. At a higher temperature above 300 °C, CO<sub>2</sub> was a main oxidized product and CO<sub>x</sub> selectivity was increased to 62.2% whereas the selectivity to oxygenates was suppressed to 32.7% with the significantly enhanced rates of CH<sub>4</sub> and N<sub>2</sub>O conversion with the values of 7.18 to 14.21 mmol/(g<sub>cat</sub>·h). The formed hydrocarbons were found to be mainly C<sub>2</sub>-C<sub>3</sub> olefins, which seems to be attributed to the active  $\alpha$ -oxygen species originated from a radical decomposition of N<sub>2</sub>O through a possible oxidative coupling of methane. At the much higher temperature of 360 °C, the fully combusted CO<sub>x</sub> selectivity was increased to 88.3% with a lower selectivity to hydrocarbons and oxygenates. The effects of feed composition of CH<sub>4</sub>/oxidant were also reported by using nonthermal plasma at ambient conditions [46,47], and the direct methane conversion to oxygenates was largely altered according to molar ratios of CH<sub>4</sub>/N<sub>2</sub>O at fixed flow rate of the reactants. By increasing a molar composition of N<sub>2</sub>O, the conversion of CH<sub>4</sub> was increased while that of N<sub>2</sub>O was decreased and the selectivity to oxygenates such as methanol and formaldehyde was decreased whereas the amount of CO<sub>x</sub>

was increased dramatically as well. Therefore, the abundant presence of active  $\alpha$ -oxygen species with a relatively higher decomposition rate compared with those of  $\text{CH}_4$  can be responsible for a higher selectivity to fully oxidized  $\text{CO}_x$  formation instead of oxygenates.

From the results of  $\text{N}_2\text{O}$  titration as summarized in **Table 1**, the rate of  $\text{N}_2\text{O}$  conversion was not directly proportional to total number of  $\alpha$ -oxygen sites on the Fe/zeolites, however, the consumed amount of  $\text{N}_2\text{O}$  was related to the number of those sites, which showed a higher value on the Fe/FeR than Fe/ZSM-5. During the reaction, the reactive oxygen species by  $\text{N}_2\text{O}$  decomposition can be adsorbed on the partially reduced iron nanoparticles which were named as  $\alpha$ -oxygen sites. Since this  $\alpha$ -oxygen can activate the adsorbed  $\text{CH}_4$  molecule,  $\text{CH}_4$  can be dissociated to form methoxy and hydroxyl species on the oxidized  $\text{Fe}^{3+}$  sites, and the methoxy species can be migrated to Si sites by forming methanol selectively on the Bronsted acid sites [19,28]. These reaction schemes were proposed by in-situ FT-IR characterization for the reaction of  $\text{CH}_4$  and  $\text{N}_2\text{O}$  on the Fe/MFI catalyst previously [48]. The adsorbed  $\text{CH}_3\text{OH}$  intermediates on the acid sites can be further reacted with another methoxy group or methanol to DME by successive dehydration reaction as well [49]. Therefore, not only the formation of methoxy groups on the  $\alpha$ -oxygen sites but also the amount of hydroxyl groups of the Bronsted acid sites seems to be important for the formation of methanol and DME from an adsorbed  $\text{CH}_4$  and  $\text{N}_2\text{O}$ . The amount of surface hydroxyl groups, which were mainly originated from Bronsted acid sites of the Fe/zeolites, is also important for a formation of  $\alpha$ -oxygen sites [24,29,30]. By changing the location of iron species during catalyst preparation, the amount of unoccupied Bronsted acid sites can be adjusted by controlling the size of iron nanoparticles and the amount of  $\alpha$ -oxygen sites as well. In addition, an excess dehydration of the oxygenates on the Fe/ZSM-5 seems to be responsible for forming olefinic hydrocarbons through a well-known MTO reaction pathway, and the dehydration of oxygenates to olefinic hydrocarbons can occur on the strong Bronsted acid sites which finally transformed to coke

precursors. From the results of slight catalyst deactivation with time on stream as shown in **Figure 3**, it was observed that the selectivity to olefinic hydrocarbons and CO<sub>x</sub> was steadily decreased. This activity variation seems to be attributed to coke formation on the strong acid sites by lessening the dehydration activity of oxygenates to hydrocarbons through a well-known carbon pool mechanisms [28-30,49]. Therefore, the strength and amount of the surface hydroxyl groups associated with Bronsted acid sites on the Fe/zeolites can change the rate of CH<sub>4</sub> conversion and product distribution by altering dehydration activity of the oxygenated intermediates on the Fe/zeolites. For a brief comparison with present Fe/FER catalytic system with others, the characteristics and activities of various heterogeneous catalysts to utilize CH<sub>4</sub> and N<sub>2</sub>O (or H<sub>2</sub>O<sub>2</sub>) oxidant to form oxygenates selectively are summarized in **Table 3**, and a higher formation rate of oxygenates such as DME and methanol was observed on the present Fe/FER(IMP).

### 3.3. Active sites for a direct CH<sub>4</sub> activation with different product distribution

To confirm the proposed reaction schemes and different catalytic performances during direct activation of CH<sub>4</sub> with the help of N<sub>2</sub>O, the  $\alpha$ -oxygen sites and the amount of acid sites with the types such as Bronsted and Lewis sites on the Fe/zeolites were quantitatively measured by the characterizations of N<sub>2</sub>O titration, NH<sub>3</sub>-TPD and Py-IR analysis. The results of NH<sub>3</sub>-TPD and Py-IR analysis are displayed in **Figure 4** and **Figure 5**, and the results are summarized in **Table 1**. As shown in **Figure 4**, three major desorption peaks of NH<sub>3</sub> on the Fe/zeolites were observed at maximum peak temperatures at around 180, 400 and 500 °C. These desorption peaks can be assigned to the weak, strong acid sites and water desorption by a formation of water from surface hydroxyl groups of zeolite frameworks [41,42,50-55]. The much larger peak intensity of the weak acid sites was observed on the Fe/FER than the Fe/ZSM-5 due to a lower Si/Al ratio of FER than ZSM-5 with intrinsically larger amount of weak acid sites on

the FER [39,53,54]. The number of weak and strong acid sites was further calculated by deconvoluting the broad desorption peaks of  $\text{NH}_3$ , and the results are summarized in **Table 1**. By comparing with the acid sites of the unmodified bare zeolites, the number of weak acid sites after Fe modification on the zeolites was increased and vice versa of the strong acid sites. The respective values of weak and strong acid sites on the bare ZSM-5 were found to be of 0.145 and 0.594 mmol  $\text{NH}_3/\text{g}$  and those values of 0.541 and 0.400 mmol  $\text{NH}_3/\text{g}$  on the FER. The decreased amount of the strong acid sites after Fe modification with the respective values of 0.417 and 0.375 mmol  $\text{NH}_3/\text{g}$  on the Fe/ZSM-5(IMP) and Fe/ZSM-5(IE) and those of 0.362 and 0.253 mmol  $\text{NH}_3/\text{g}$  on the Fe/FER(IMP) and Fe/FER(IE) was attributed to the selective ion-exchange of iron nanoparticles on the strong acid sites [52-54]. In addition, an increased amount of the weak acid sites with the respective values of 0.206 and 0.255 mmol  $\text{NH}_3/\text{g}$  on the Fe/ZSM-5(IMP) and Fe/ZSM-5(IE) and those of 0.545 and 0.554 mmol  $\text{NH}_3/\text{g}$  on the Fe/FER(IMP) and Fe/FER(IE) seems to be attributed to the newly formed interaction of iron oligomers with the protons of the Bronsted acid sites of zeolites.

A relative amount and type of the acid sites of the Fe/zeolites were further characterized by Py-IR and the absorption peaks of pyridine molecules are displayed in **Figure 5**. Three characteristic absorption bands of pyridine molecules were clearly observed by the adsorption of pyridine on Bronsted (B), Lewis (L) and combined acid sites of the Fe/zeolites. The absorption band located at around  $1450\text{ cm}^{-1}$  was attributed to Lewis acid sites for C-C stretching vibration mode of the adsorbed pyridine complex. The absorption band at around  $1540\text{ cm}^{-1}$  was attributed to C-C stretching vibration of the pyridinium ions adsorbed on the Bronsted acid sites, and the peak at around  $1490\text{ cm}^{-1}$  is assigned to the interaction of pyridine molecules on both Lewis and Bronsted acid sites as well [55]. To verify separate amounts of Bronsted and Lewis acid sites on the Fe/zeolites, the integrated area of the each peak at  $1540\text{ cm}^{-1}$  was divided by that of  $1450\text{ cm}^{-1}$  which is denoted as B/L ratio, and the

results are summarized in **Table 1**. The B/L ratio was also calculated on the unmodified bare zeolites and the values were found to be 8.3 and 74.0 on the ZSM-5 and FER, respectively. The B/L ratio was decreased after Fe modification on both zeolites by showing the values of 3.6 and 1.7 on the Fe/ZSM-5(IMP) and Fe/ZSM-5(IE) and those of 32.8 and 21.5 on the Fe/FER(IMP) and Fe/FER(IE), respectively. From the Py-IR results, the number of Bronsted acid sites on the Fe/FER(IMP) was found to be larger than other Fe/zeolites and the catalytic activity was found to be higher on the Fe/FER(IMP) having a larger amount of Bronsted acid sites because Bronsted acid sites are known to be most active sites for methanol dehydration reaction [52-54]. Therefore, a larger amount of weak Bronsted acid sites with abundant  $\alpha$ -oxygen sites can be responsible for a higher methane conversion rate on the Fe/FER and a lower conversion rate seems to be attributed to a lower amount of Bronsted acid sites with strong acidity on the Fe/ZSM-5 through the MTO reaction pathway which can lead to form severe coke precursors as well [56].

The decomposition activity of  $N_2O$  as a mild oxidizing agent can be strongly affected by total amount of  $\alpha$ -oxygen sites on the Fe/zeolites. Therefore, the quantity of active  $\alpha$ -oxygen sites was measured by a pulse  $N_2O$  chemisorption and the amount of  $\alpha$ -oxygen sites is summarized in **Table 1**. The much smaller amount of  $\alpha$ -oxygen sites was observed on the Fe/ZSM-5(IMP) with the value of  $1.8 \times 10^{19}$  molecules/g than the Fe/FER(IMP) with  $10.3 \times 10^{19}$  molecules/g. In addition, a smaller amount of  $\alpha$ -oxygen sites was also observed on the Fe/ZSM-5(IE) with the value of  $0.7 \times 10^{19}$  molecules/g than that of  $10.0 \times 10^{19}$  molecules/g on the Fe/FER(IE), and the Fe/FER showed almost ten times larger amount of  $\alpha$ -oxygen sites than the Fe/ZSM-5. In general, the active  $\alpha$ -oxygen sites can be formed by redox cycles of two iron cations through a transformation of  $Fe^{3+} \leftrightarrow Fe^{2+}$ , which are attached to ion-exchanged iron sites closely bridged with an oxygen atoms by a decomposition of  $N_2O$  [51]. Since FER zeolite has a shorter distance and easy accessibility between ion-exchanged  $\alpha$ -iron

cations than that of ZSM-5, the shorter distance between ion-exchanged iron cations on the FER may increase a probability of active  $\alpha$ -oxygen formation. Furthermore,  $\alpha$ -iron cations are located on the pore channel of 10-membered ring with a pore size of 0.42 x 0.54 nm, whereas the ZSM-5 has slightly larger pore size of 0.54 x 0.56 nm of 10-membered ring with zigzag pore structures intersecting the straight pore channel with a longer distance between ion-exchanged iron cations [17,50,51]. These positive structural properties of the FER can enhance the decomposition rate of N<sub>2</sub>O [38], and it can enhance a rate of CH<sub>4</sub> activation possibly. However the active  $\alpha$ -oxygen sites on the Fe/ZSM-5 have not been intimately faced due to the characteristic zigzag pore structures of the ZSM-5, and N<sub>2</sub>O decomposition seems to be difficult on the Fe/ZSM-5 compared to the Fe/FER.

Even though a loading amount of iron precursor was found to be lower on the Fe/ZSM-5(IE) and Fe/FER(IE) with the respective values of 4.8 and 6.4 wt% than those of 7.8 and 7.3 wt% on the Fe/ZSM-5(IMP) and Fe/FER(IMP), the amount of  $\alpha$ -iron sites was found to be larger on the Fe/FER than the Fe/ZSM-5 especially on the Fe/zeolites prepared by impregnation method. From the results of N<sub>2</sub>O titration, the amount of active  $\alpha$ -oxygen sites was slightly larger on the Fe/FER(IMP) than the Fe/FER(IE) as well. As shown in **Figure 6**, TEM images of the selected Fe/FER(IMP) and Fe/FER(IE) after reaction showed a significant aggregation of the iron oxide nanoparticles (magnified images in the inset figures). The fresh Fe/FER(IE) showed well-dispersed iron nanoparticles with a particle size of below 10 nm because of the selective adsorption of iron precursor to the Bronsted acid sites, however, the iron oxide nanoparticles were significantly aggregated on the used Fe/FER(IE) with a particle size above 50 nm. Interestingly, the iron oxide nanoparticles with a heterogeneous size distribution in the range of 10 – 50 nm in size were clearly observed on the fresh Fe/FER(IMP). On the used Fe/FER(IMP), the aggregation of iron nanoparticles was found to be more significant than that of the Fe/FER(IE), which suggests a less number of iron nanoparticles blocks the active

Bronsted acid sites compared with the Fe/FER(IE). This observation can explain a slightly higher selectivity to DME on the Fe/FER(IMP) than Fe/FER(IE) due to largely exposed active acid sites for methanol dehydration to DME [39,49,53,54,57,58]. In addition, a larger iron oxide nanoparticles on the Fe/FER(IMP), which are active sites by forming  $\alpha$ -oxygen sites, can enhance the fully oxidized CO<sub>x</sub> products through a facile oxidation of intermediates, especially on the Fe/FER compared to the Fe/ZSM-5. In addition, the deposited coke precursors can also change the catalytic activity and product distribution by blocking the active sites such as  $\alpha$ -oxygen sites and Bronsted acid sites mainly. Even though a filamentous coke formation was not clearly observed even in the magnified TEM images on the used Fe/FER, the extent of coke formation was confirmed by hydrogenation of cokes through TPSR. As shown in **Figure 7**, TPSR experiment showed that the deposited coke precursors were hydrogenated to form CH<sub>4</sub> under a flow of H<sub>2</sub>, which was verified by peaks of the m/z values of 15 and 14 on the used Fe/ZSM-5 and Fe/FER. The amount of coke formation was much larger on the used Fe/ZSM-5 than the Fe/FER irrespective to the preparation methods, which revealed the coke deposition also altered the product distribution and the rate of CH<sub>4</sub> conversion as well. The formed coke precursors seem to be much dominant on the Fe/ZSM-5 having stronger acid sites due to a facile reaction pathway through MTO reaction. The amount of coke deposition on acid sites and  $\alpha$ -oxygen sites was well correlated with catalytic performances, and we proposed a possible reaction pathway and schemes based on the product distribution with respect to acid sites and  $\alpha$ -oxygen sites in **Figure 8** and **Scheme 1**.

### 3.4. Proposed reaction pathway for the formation of oxygenates and hydrocarbons

To further verify the effect of acidic properties and  $\alpha$ -oxygen sites on the Fe/ZSM-5 and Fe/FER for a different product distribution, methanol conversion reaction to oxygenates and hydrocarbons was further carried out under an environment of N<sub>2</sub>O flow with a feeding of

liquid methanol and the results are summarized in supplementary **Table S3**. For a methanol conversion to hydrocarbons by MTO reaction pathway, methanol can be previously dehydrated to DME, and it can be transformed to a broad range of hydrocarbons including light olefins such as C<sub>2</sub> - C<sub>4</sub> hydrocarbons through carbon pool mechanisms [59-61]. In addition, methanol conversion with stability and product distribution are strongly depending on the surface acidic properties such as the number of acid sites and their strengths [60,61]. As shown in supplementary **Table S3**, the bare ZSM-5 and FER showed a similar conversion of methanol with a value of 87.7% on the ZSM-5 and 87.4% on the FER. However, a significantly different product distribution was observed by showing a higher hydrocarbon selectivity of 51.3% on the ZSM-5 and a higher DME selectivity of 99.8% on the FER. Based on the acidic properties of the Fe/zeolites as summarized in **Table 1** from NH<sub>3</sub>-TPD and Py-IR, the observed higher conversion of methanol and DME selectivity on the bare FER can be attributed to a larger amount of Bronsted acid sites, and vice versa on the ZSM-5 by showing a higher selectivity to hydrocarbons due to a large amount of strong acid sites. On the ZSM-5, conversion of methanol seems to follow a well-known auto-catalyzed reaction on the strong acid sites through a consecutive transformation of DME to hydrocarbons [59]. However, after Fe modification on the zeolites, methanol conversion was decreased due to a suppressed amount of Bronsted acid sites, which was more significant on the Fe/ZSM-5(IE) and Fe/FER(IE) than the Fe/ZSM-5(IMP) and Fe/FER(IMP). This can be attributed to a well distributed iron oxide nanoparticles on the acid sites of the zeolites through an ion-exchange as confirmed by TEM analysis. Interestingly, the selectivity to hydrocarbons on the Fe/ZSM-5 was significantly suppressed due to a selective adsorption of iron species on the strong acid sites as well [52-54,59]. However, the product distribution showed that the selectivity to oxygenates was above 90% on all Fe-modified zeolites. The selectivity to oxygenates can be largely increased from 48.7 % on the bare ZSM-5 up to 97% with a small amount of

hydrocarbon formation on the Fe/ZSM-5 due to selective adsorption of  $\alpha$ -oxygen sites from iron on the strong acid sites. These results also revealed that the reaction followed a different reaction pathway compared to a general methanol dehydration by introducing  $\alpha$ -oxygen sites for methanol conversion. The reaction mainly undergoes the dehydration of methanol to DME by prohibiting the formation of carbon pools from a successive dehydration of DME on the Fe/ZSM-5. Therefore, the formation of coke precursors on the strong acidic sites by the successive dehydration of DME to hydrocarbons through carbon pool mechanisms can be largely prohibited by the assistance of  $\alpha$ -oxygen sites. The differences of the converted amount of  $N_2O$  was clearly observed on all Fe/zeolites which suggests the  $\alpha$ -oxygen site can efficiently take part in  $CH_4$  activation reaction. The  $\alpha$ -oxygen sites can also form CO product by decomposition of intermediates through a partial oxidation reaction, especially on the Fe/FER having an abundant active  $\alpha$ -oxygen sites. Compared with a direct conversion of  $CH_4$  with  $N_2O$ , a relative amount of CO formed was found to be quite small during methanol dehydration. However, hydrocarbon selectivity was still higher on the Fe/ZSM-5 than the Fe/FER. Generally,  $CO_x$  molecules can be formed by a partial oxidation of methane or surface intermediates such as adsorbed hydrocarbons or oxygenates [52,53]. Therefore, the observed larger amount of CO on the Fe/FER than the Fe/ZSM-5 during a direct activation of  $CH_4$  with  $N_2O$  can be attributed to a partial oxidation of the adsorbed intermediates due to an abundant presence of active  $\alpha$ -oxygen sites on the Fe/FER. Based on the addition reaction results, the reaction pathway of  $CH_4$  activation through  $N_2O$  decomposition with a different product distribution on the Fe/zeolites are schematically presented in **Figure 8**, and the reaction scheme is also displayed in **Scheme 1**. The Fe/ZSM-5 having a small amount of  $\alpha$ -oxygen sites with strong Bronsted acid sites showed lower  $CH_4$  and  $N_2O$  conversion with a higher selectivity to olefinic hydrocarbons and DME with a little bit higher amount of coke deposition due to an easy consecutive reaction of methanol or DME intermediates to olefinic

hydrocarbons on the strong acid sites. However, the Fe/FER having a larger amount of the  $\alpha$ -oxygen sites with a large amount of weak Bronsted acid sites can increase the rate of CH<sub>4</sub> and N<sub>2</sub>O conversion with a higher selectivity to oxygenates and CO<sub>x</sub> products. This was mainly attributed to a higher formation of methoxy groups with a large amount of Bronsted acid sites as hydroxyl supplier and a simultaneous oxidation of the adsorbed methoxy or methanol intermediates to fully oxidized CO<sub>x</sub> on active  $\alpha$ -oxygen sites of the Fe/FER as summarized in **Scheme 1**.

In summary, the activation of CH<sub>4</sub> under N<sub>2</sub>O decomposition was much easier on the Fe/FER due to the presence of a larger amount of active  $\alpha$ -oxygen sites and weak Bronsted acid sites, especially on the Fe/FER(IMP). However, the product distribution such as DME, methanol and hydrocarbons was strongly depending on the amount and strength of Bronsted acid sites through the proposed reaction pathway in **Figure 8**. The Fe/ZSM-5 having a large amount of strong acid sites seems to be responsible for a selective production of olefinic hydrocarbons and DME through a consecutive dehydration reaction of methanol (or DME) to unsaturated C<sub>2</sub>-C<sub>3</sub> hydrocarbons. Therefore, the Fe/FER having abundant Bronsted acid sites seems to be a proper catalytic system to obtain oxygenates such as methanol and DME with a higher rate of CH<sub>4</sub> conversion compared to the Fe/ZSM-5. This simple controlling method of  $\alpha$ -oxygen sites and Bronsted acid sites can be applied to obtain a higher rate of CH<sub>4</sub> conversion and selectivity to oxygenates for a direct CH<sub>4</sub> activation with N<sub>2</sub>O decomposition.

#### 4. Conclusions

For a direct activation of CH<sub>4</sub> under N<sub>2</sub>O decomposition to oxygenates such as methanol and DME as well as light olefinic hydrocarbons on the Fe-modified ZSM-5 and FER, the amount of active  $\alpha$ -oxygen sites and weak Bronsted acid sites are crucial factors to alter CH<sub>4</sub> conversion and product distribution as well. A facile activation of CH<sub>4</sub> with N<sub>2</sub>O

decomposition was found to be more significant on the Fe/FER prepared by impregnation method due to an abundant presence of active  $\alpha$ -oxygen sites as well as weak Bronsted acid sites. The Fe/ZSM-5 having a large amount of strong acid sites was also responsible for a higher selectivity to unsaturated C<sub>2</sub>-C<sub>3</sub> hydrocarbons and DME with a little bit higher coke deposition. However, the Fe/FER having a large amount of the weak Bronsted acid sites was found to be proper for obtaining oxygenates such as methanol and DME. Therefore, the main controlling variables for catalytic performances during direct CH<sub>4</sub> activation with the help of N<sub>2</sub>O decomposition can be the amount of active  $\alpha$ -oxygen sites with a different distribution of iron oxide nanoparticles and the Bronsted acid sites with their strength, which were strongly altered by preparation methods.

### **Acknowledgements**

This work was also financially supported by an institutional program grant (2E26570-16-037) from the Korean Institute of Science and Technology (KIST) and by Fundamental Research Program of the Korea Institute of Materials Science (PNK4310). The authors would like to acknowledge the financial support from the National Research Foundation of Korea (NRF) grant funded by the Korea government (NRF-2014R1A1A2A16055557 and NRF-2016M3D3A1A01913253). This work was supported by the National Research Council of Science and Technology (NST) through Degree and Research Center (DRC) Program (2015). This work was financially supported by the R&D Center for Valuable Recycling (Global-Top R&D Program) of the Ministry of Environment of Korea (Project No. RE201606017).

**References**

- [1] J.H. Lunsford, *Catal. Today* 63 (2000) 165-174.
- [2] A.B.M.L. Rahman, M. Kumashiro, T. Ishihara, *Catal. Commun.* 12 (2011) 1198-1200.
- [3] M.J. Brown, N.D. Parkyns, *Catal. Today* 8 (1991) 305-335.
- [4] N. Yuqin, C. Zhenghua, H. Xiuhua, J. Tao, P. Junxuan, L. Yu, Z. Xia, T. Yisheng, *J. Nat. Gas. Chem.* 9(2000) 59-67.
- [5] K.J. Zhen, M.M. Khan, C.H. Mak, K.B. Lewis, G.A. Somorjai, *J. Catal.* 94 (1985) 501-507.
- [6] H.F. Liu, R.S. Liu, K.Y. Liew, R.E. Johnson, J.H. Lunsford, *J. Am. Chem. Soc.* (1984), 106, 4117-4121.
- [7] X. Wang, Y. Wang, Q. Tang, Q. Guo, Q. Zhang, H. Wan, *J. Catal.* 217 (2003) 457-467.
- [8] R. Polniser, M. Stolcova, M. Hronec, M. Mikula *Appl. Catal. A:Gen.* 400 (2011) 122-130.
- [9] H. Launay, S. Loridant, A. Pigamo, J.L. Dubois, J.M.M. Millet, *J. Catal.* 246 (2007) 390-398.
- [10] S. Chempath, A.T. Bell, *J. Catal.* 247 (2007) 119-126.
- [11] S. Mansouria, O. Benlounes, C. Rabia, R. Thouvenot, M.M. Bettahar, S. Hocine, *J. Mol. Catal. A: Chem.* 379 (2013) 255-262.
- [12] N.V. Beznis, B.M. Weckhuysen, J.H. Bitter, *Catal. Lett.* 136 (2010) 52-56.
- [13] M.F. Fellah, I. Onal, *J. Phys. Chem.C* 114 (2010) 3042-3051.
- [14] J.P. Tessonier, L. Benoit, S. Rigolet, M.J. Ledoux, C. Pham-Huu, *Appl. Catal. A: Gen.* 336 (2008) 79-88.
- [15] J.P. Tessonier, L. Benoit, M.J. Ledoux, C. Pham-Huu, *Catal. Commun.* 8 (2007) 1787-1792.
- [16] C. Hammond, M.M. Forde, M.H.A. Rahim, A. Thetford, Q. He, R.L. Jenkins, N. Dimitratos, J.A. Lopez-Sanchez, N.F. Dummer, D.M. Murphy, A.F. Carley, S.H. Taylor, D.J.

Willock, E.E. Stangland, J. Kang, H. Hagen, C.J. Kiely, G.J. Hutchings, *Angew. Chem. Int. Ed.* 51 (2012) 5129-5133.

[17] P. Pantu, B. Boekfa, B. Sunpetch, J. Limtrakul, *Chem. Eng. Comm.* 195 (2008) 1477-1485.

[18] A. Heyden, N. Hansen, A.T. Bell, F.J. Keil, *J. Phys. Chem. B* 110 (2006) 17096-17114.

[19] E.V. Starokon, M.V. Parfenov, L.V. Pirutko, S.I. Abornev, G.I. Panov, *J. Phys. Chem. C* 115 (2011) 2155-2161.

[20] J. Xu, R.D. Armstrong, G. Shaw, N.F. Dummer, S.J. Freakley, S.H. Taylor, G.J. Hutchings, *Catal. Today* 270 (2016) 93-100.

[21] Y.F. Chang, J.H. McCarty, *Catal. Lett.* 34(1995) 163-177.

[22] B.R. Wood, J.A. Reimer, A.T. Bell, M.T. Janicke, K.C. Ott, *J. Catal.* 224 (2004) 148-155.

[23] C. Sang, B.H. Kim, Carl R.F. Lund, *J. Phys. Chem. B* 109 (2005) 2295-2301.

[24] E.V. Starokon, K.A. Dubkov, L.V. Pirutko, G.I. Panov, *Top. Catal.* 23 (2003) 137-143.

[25] L. Kiwi-Minsker, D.A. Bulushev, A. Renken, *J. Catal.* 219 (2003) 273-285.

[26] G.I. Panov, A.K. Uriarte, M.A. Rodkin, V.I. Sobolev, *Catal. Today* 41 (1998) 365-385.

[27] P.J. Smeets, J.S. Woertink, B.F. Sels, E.I. Solomon, R.A. Schoonheydt, *Inorg. Chem.* 49 (2010) 3573-3583.

[28] M.V. Parfenov, E.V. Starokon, L.V. Pirutko, G.I. Panov, *J. Catal.* 318 (2014) 14-21.

[29] L.V. Pirutko, V.S. Chernyavsky, A.K. Uriarte, G.I. Panov, *Appl. Catal. A: Gen.* 227 (2002) 143-157.

[30] P.P. Notte, *Top. Catal.* 13 (2000) 387-394.

[31] R.J. Madon, M. Boudart, *Ind. Eng. Chem. Fundam.* 21 (1982) 438-447.

[32] A.Y. Khodakov, W. Chu, P. Fongarland, *Chem. Rev.* 107 (2007) 1692-1744.

[33] D. Verboekend, R. Caicedo-Realpe, A. Bonilla, M. Santiago, J. Peerez-Ramirez, *Chem. Mater.* 22 (2010) 4679-4689.

- [34] F. Zhang, X. Chen, J. Zhuang, Q. Xiao, Y. Zhong, W. Zhu, *Catal. Sci. Technol.* 1 (2011) 1250-1255.
- [35] X. Cheng, J. Wang, J. Guo, J. Sun, Y. Long, *Chem. Phys. Chem.* 7 (2006) 1198-1202.
- [36] M.S. Batista, M. Wallau, E.A. Urquieta-Gonzalez, *Brazilian J. Chem. Eng.* 22 (2005) 341-351.
- [37] J. Perez-Ramírez, *J. Catal.* 227 (2004) 512-522.
- [38] L.Li, Q. Shen, J. Li, Z. Hao, Z.P. Xu, G.Q. Max Lu, *Appl. Catal. A: Gen.* 344 (2008) 131-141.
- [39] S.H. Kang, J.H. Ryu, J.H. Kim, I.H. Jang, A.R. Kim, G.Y. Han, J.W. Bae, K.S. Ha, *Energy Fuels* 26 (2012) 6061-6069.
- [40] M. Mihaylov, E. Ivanova, N. Drenchev, K. Hadjiivanov, *J. Phys. Chem. C* 114 (2010) 1004-1014.
- [41] L.J. Lobree, I.C. Hwang, J.A. Reimer, A.T. Bell, *J. Catal.* 186 (1999) 242-253.
- [42] E.M. El-Malki, R.A. van Santen, W.M.H. Sachtler, *J. Phys. Chem.* 103 (1999) 4611-4622.
- [43] A. Guzman-Vargas, G. Delahay, B. Coq, *Appl. Catal. B: Environ.* 42 (2003) 369-379.
- [44] H.Y. Chen, W.M.H. Sachtler, *Catal. Today* 42 (1998) 73-83.
- [45] M.H. Jeong, D.H. Lee, J.W. Bae, *Int. J. Hydrogen Energy* 40 (2015) 2613-2620.
- [46] Sk. Mahammadunnisa, P.M.K. Reddy, Ch. Subrahmanyam, *RSC Adv.* 4 (2014) 4034-4036.
- [47] Sk. Mahammadunnisa, K. Krushnamurty, Ch. Subrahmanyam, *Catal. Today* 256 (2015) 102-107.
- [48] B.R. Wood, J.A. Reimer, A.T. Bell, M.T. Janicke, K.C. Ott, *J. Catal.* 225 (2004) 300-306.
- [49] K.S. Ha, Y.J. Lee, J.W. Bae, Y.W. Kim, M.H. Woo, H.S. Kim, M.J. Park, K.W. Jun,

Appl. Catal. A: Gen. 395 (2011) 95-106.

[50] W. Junying, X. Haian, J. Xiaohua, F. Fengtao, F. Zhaochi, L. Can, Chin. J. Catal. 34 (2013) 876-888.

[51] J. Dedecek, D. Kaucky, B. Wichterlova, Top. Catal. 18 (2002) 283-290.

[52] L. Ma, H. Qu, J. Zhang, Q. Tang, S. Zhang, Q. Zhong, Res. Chem. Intermed. 39 (2013) 4109-4120.

[53] J.W. Bae, S.H. Kang, Y.J. Lee, K.W. Jun, Appl. Catal. B: Environ. 90 (2009) 426-435.

[54] J.W. Jung, Y.J. Lee, S.H. Um, P.J. Yoo, D.H. Lee, K.W. Jun, J.W. Bae, Appl. Catal. B: Environ. 126 (2012) 1-8.

[55] F. Jin, Y. Li, Catal. Today 145 (2009) 101-107.

[56] Y.J. Lee, Y.W. Kim, K.W. Jun, N. Viswanadham, J.W. Bae, H.S. Park, Catal. Lett. 129 (2009) 408-415.

[57] S.H. Kang, J.W. Bae, K.W. Jun, H.S. Potdar, Catal. Commun. 9 (2008) 2035-2039.

[58] S.M. Kim, Y.J. Lee, J.W. Bae, H.S. Potdar, K.W. Jun, Appl. Catal. A: Gen. 348 (2008) 113-120.

[59] N.Y. Chen, W.J. Reagan, J. Catal. 59 (1979) 123-129.

[60] S. Jiang, J.S. Hwang, T. Jin, T. Cai, W.I. Cho, Y.S. Baek, S.E. Park, Bull. Korean Chem. Soc. 25 (2004) 185-189.

[61] J.W. Park, G. Seo, Appl. Catal. A: Gen. 356 (2009) 180-188.

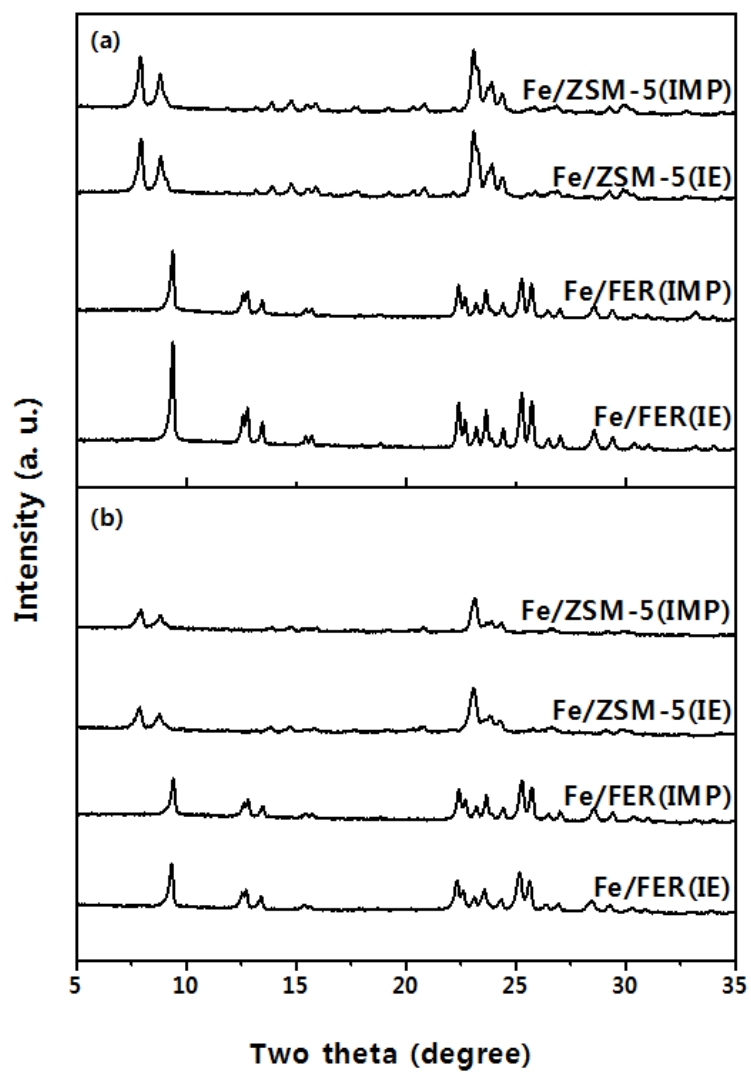


**Figure 1.** X-ray diffraction (XRD) patterns of the Fe/ZSM-5 and Fe/FER (a) before and (b) after reaction

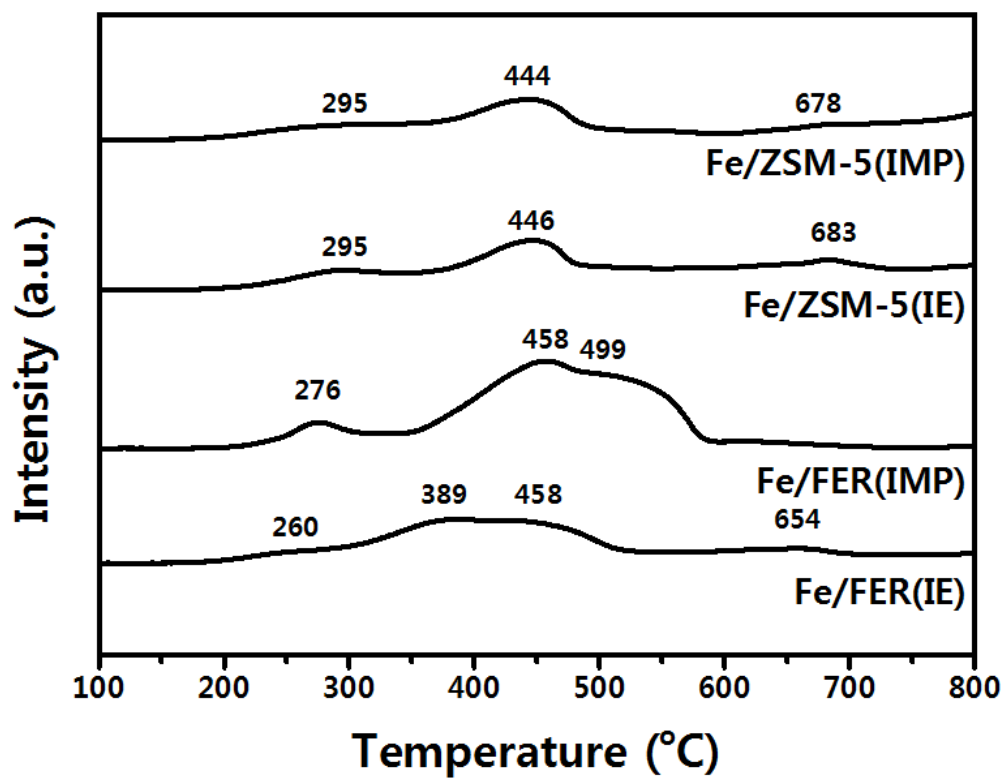


**Figure 2.** Temperature-programmed reduction (TPR) profiles of the fresh Fe/ZSM-5 and Fe/FER

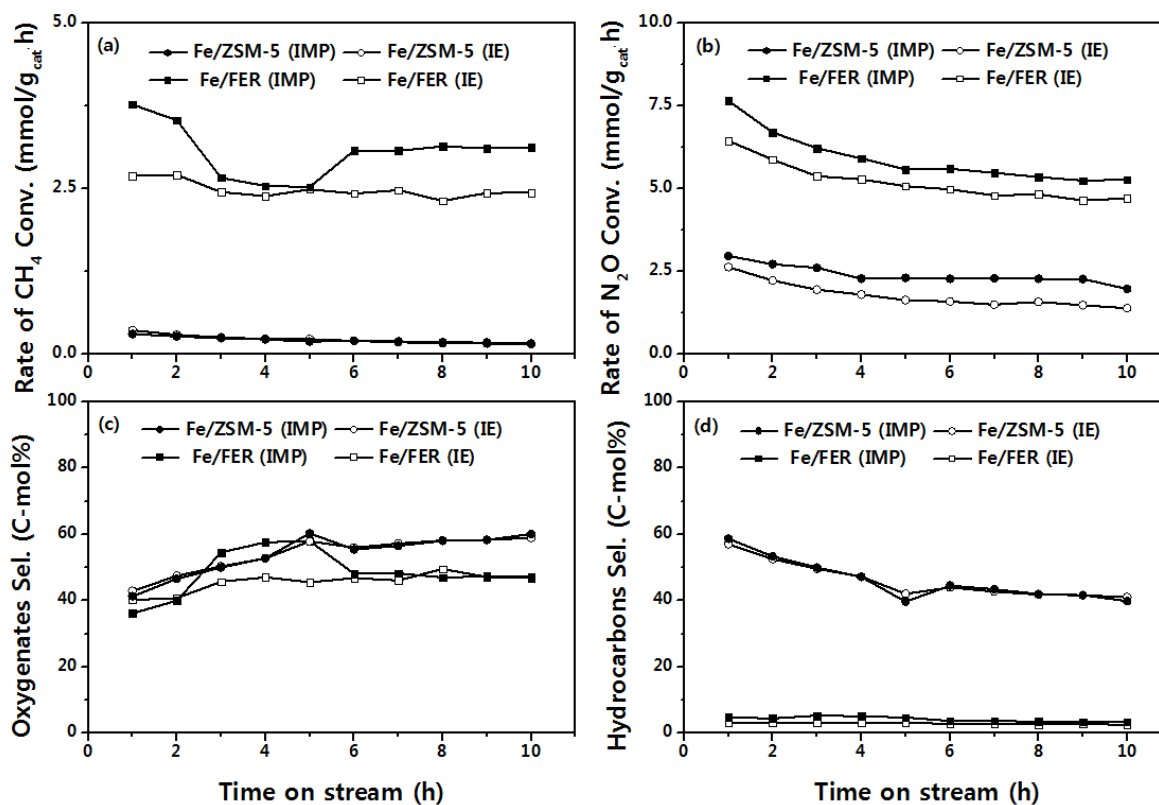


**Figure 3.** Catalytic activity with time on stream of partial oxidation of methane in the Fe/zeolites (a) rate of CH<sub>4</sub> conversion (mmol/(g<sub>cat</sub>·h)), (b) rate of N<sub>2</sub>O conversion (mmol/(g<sub>cat</sub>·h)), (c) Oxygenates selectivity at the reaction conditions: T=280 °C, P=0.1 MPa, SV=12000 mL/(g<sub>cat</sub>·h) of mixed gas (CH<sub>4</sub>/N<sub>2</sub>O=2.5 with 5vol% He)

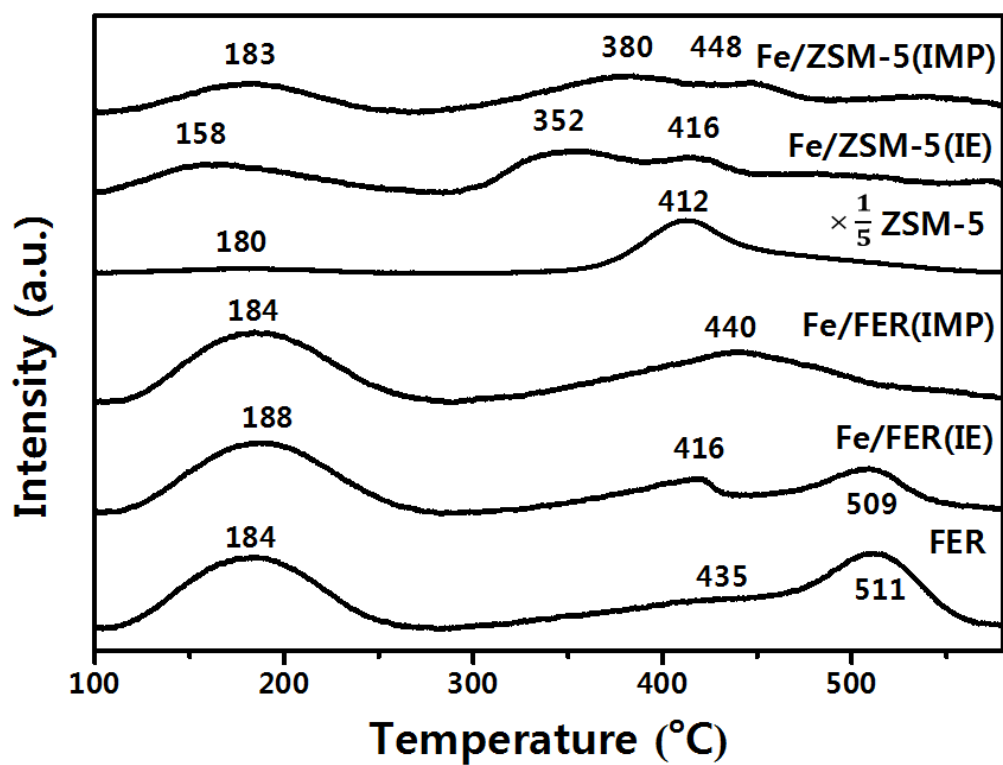


**Figure 4.** Temperature-programmed desorption of ammonia (NH<sub>3</sub>-TPD) profiles of the fresh Fe/ZSM-5 and Fe/FER with bare ZSM-5 and FER

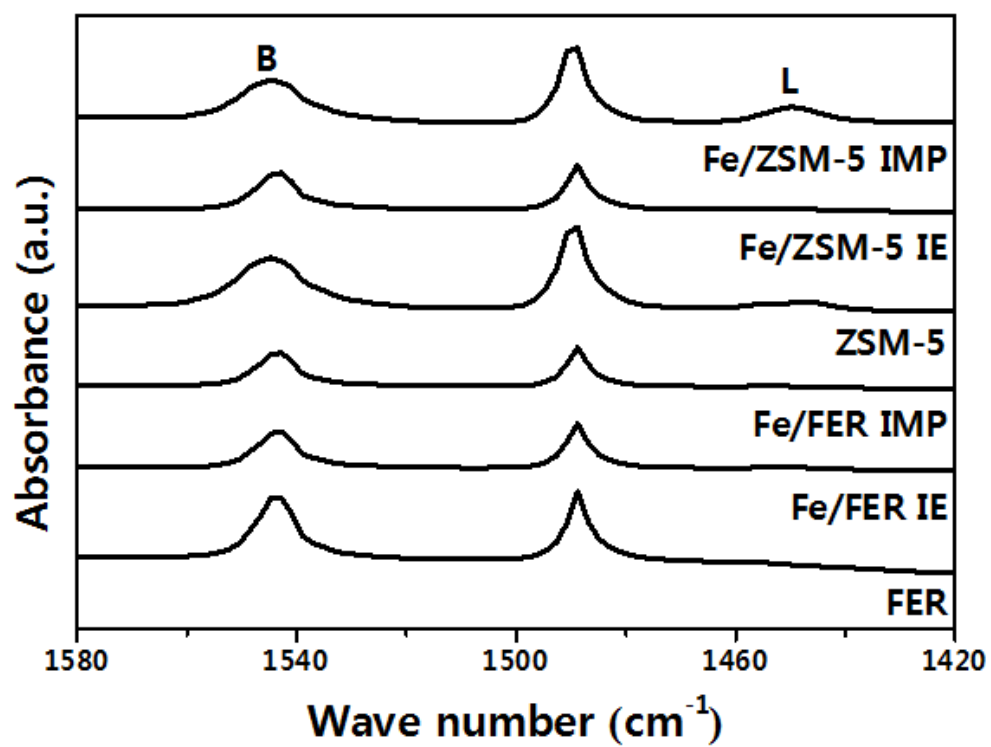


**Figure 5.** Pyridine-adsorbed FT-IR spectra on the fresh Fe/ZSM-5 and Fe/FER

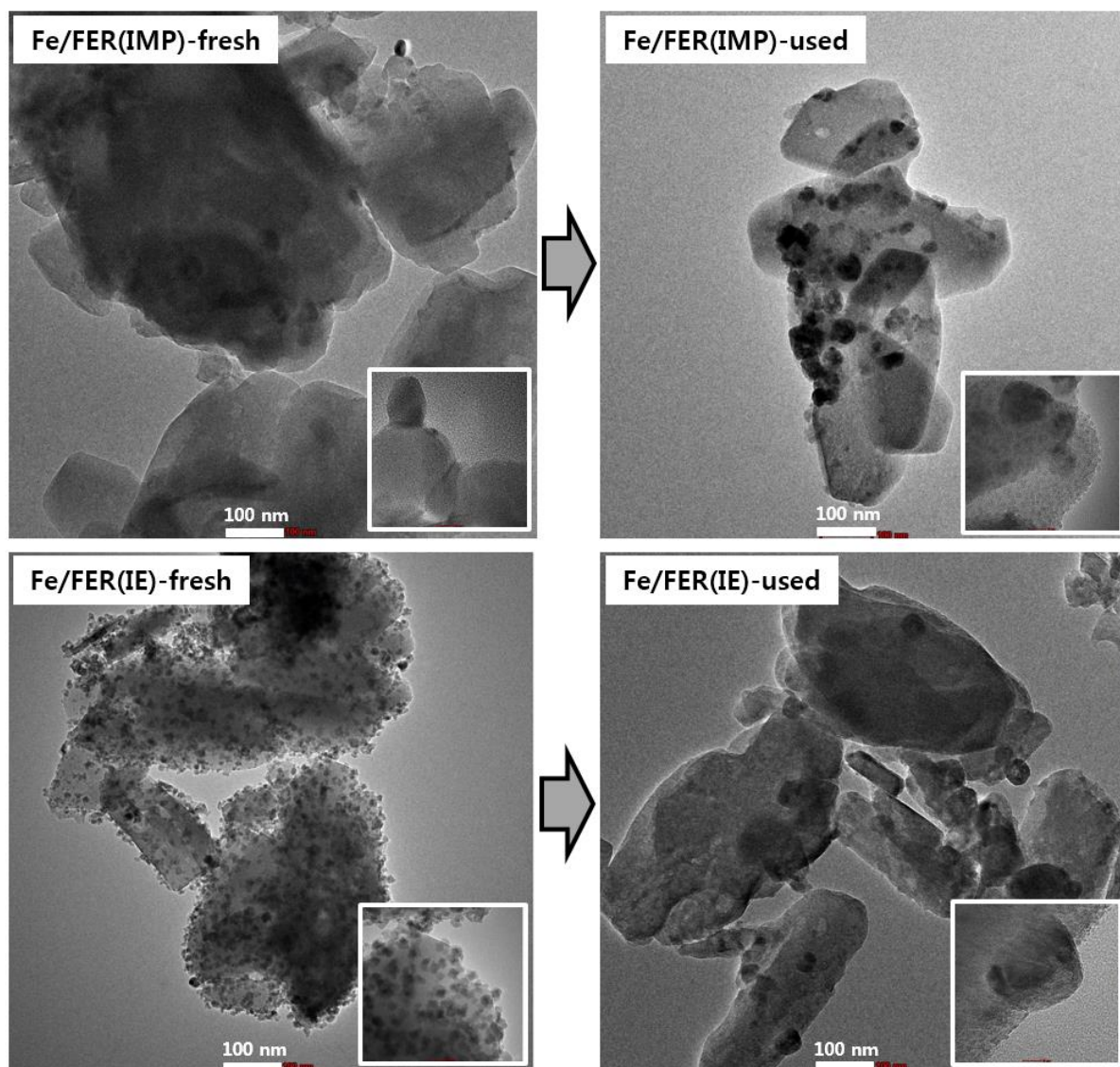


**Figure 6.** TEM images of the FER(IMP) and FER(IE) before and after reaction

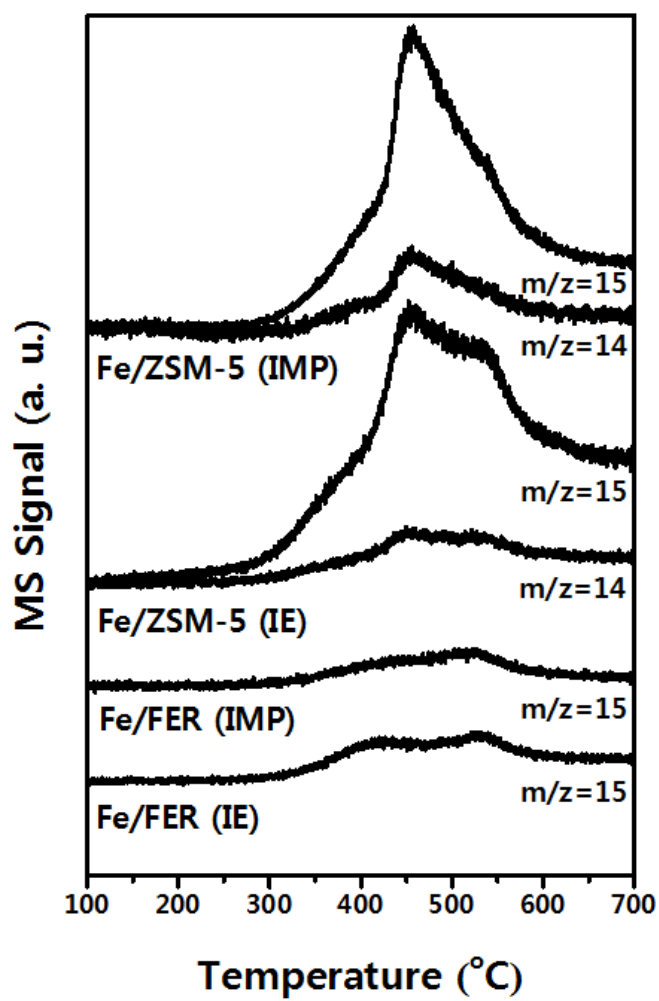


**Figure 7.** Temperature-programmed surface reaction (TPSR) profiles of used Fe/zeolites.

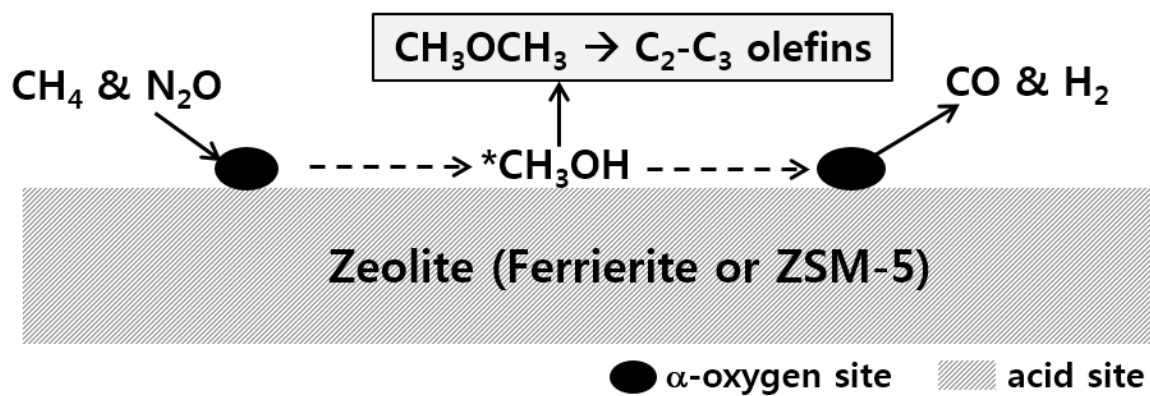
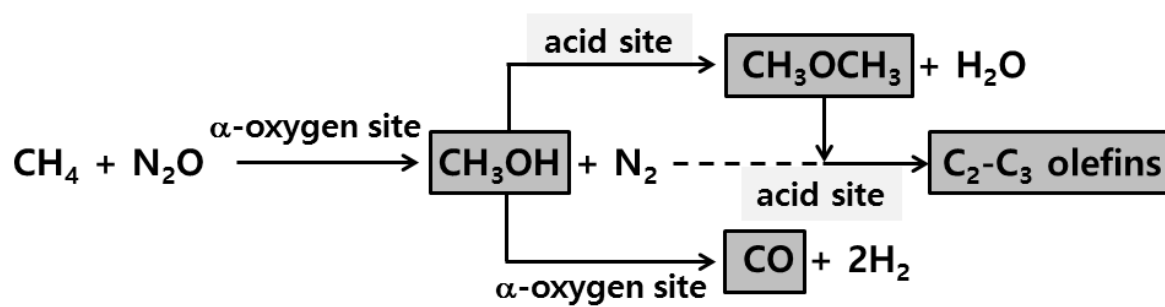


**Figure 8.** Proposed reaction pathway of a direct  $\text{CH}_4$  activation with  $\text{N}_2\text{O}$  to oxygenates and hydrocarbons on active  $\alpha$ -oxygen sites and Bronsted acid sites



**Scheme 1.** Proposed reaction schemes of a direct  $\text{CH}_4$  activation with  $\text{N}_2\text{O}$  to oxygenates and hydrocarbons

**Table 1.** Physicochemical properties of the Fe-modified zeolites

Catalyst	XRF		XRD		N <sub>2</sub> O titration	NH <sub>3</sub> -TPD	Py-IR
	Si/Al	Fe <sup>a</sup> (wt%)	Crystallinity (fresh/used) <sup>b</sup>	Variations crystallinity (%) <sup>c</sup>	of $\alpha$ -oxygen sites (x10 <sup>19</sup> molecules/g)	Acid sites (mmolNH <sub>3</sub> /g) <sup>d</sup>	(weak/strong) B/L ratio <sup>e</sup>
Fe/ZSM-5(IMP)	27.8	7.8	35 / 15	57.1	1.8	0.206 / 0.417	3.6
Fe/ZSM-5(IE)	26.2	4.8	36 / 18	50	0.7	0.255 / 0.375	1.7
ZSM-5	27.7	-	100	-	-	0.145 / 0.594	8.3
Fe/FER(IMP)	9.8	7.3	44 / 30	31.8	10.3	0.545 / 0.362	32.8
Fe/FER(IE)	10.5	6.4	72 / 37	48.6	10.0	0.554 / 0.253	21.5
FER	9.4	-	100	-	-	0.541 / 0.400	74.0

<sup>a</sup>Fe content is presented in wt% based on the total weight of Fe-modified zeolites such as ZSM-5 and FER.

<sup>b</sup>The crystallinity of Fe-modified zeolites was calculated from the ratio of the integrated area of the diffraction peaks at  $2\theta = 6 - 10^\circ$  and  $8 - 10^\circ$  to the values of the parent zeolites such as ZSM-5 and FER on the fresh and used catalysts.

<sup>c</sup>The relative crystallinity of the used Fe/zeolites was calculated based on those of the fresh Fe/zeolites.

<sup>d</sup>The maximum desorption peaks of the adsorbed NH<sub>3</sub> at around 180 and 400 °C from NH<sub>3</sub>-TPD analysis were assigned to weak and strong acid sites, respectively.

<sup>e</sup>The ratio of Bronsted (B) to Lewis (L) acid sites was calculated by dividing the integrated area of the peak assigned to the absorption band of 1450 by that of 1550 cm<sup>-1</sup>, respectively.

**Table 2.** Catalytic activities of the Fe-modified zeolites for a direct CH<sub>4</sub> activation to oxygenates and hydrocarbons<sup>a</sup>

Catalyst	Rate of conversion (mmol/(g <sub>cat</sub> ·h))		Product distribution (mol %)				
	CH <sub>4</sub>	N <sub>2</sub> O	Oxygenates			Hydrocarbons <sup>c</sup>	CO / CO <sub>2</sub>
			DME	Methanol	Others <sup>b</sup>		
Fe/ZSM-5(IMP)	0.19	2.29	37.6	20.1	0.1	42.2	0 / 0
Fe/ZSM-5(IE)	0.17	1.52	42.1	15.4	0.2	42.3	0 / 0
Fe/FER(IMP)	3.11	5.40	27.9	19.6	0.1	3.5	48.9 / 0
Fe/FER(IE)	2.42	4.80	25.8	21.4	0.1	2.6	50.1 / 0

<sup>a</sup>The catalytic activity was measured at the reaction conditions of T = 280 °C, P = 0.1 MPa, molar ratio of CH<sub>4</sub>/N<sub>2</sub>O = 2.5 and space velocity (SV) = 12000 L/(kg<sub>cat</sub>·h) for 10 h, and the products were analyzed by using an in-situ gas chromatography equipped with TCD and FID.

<sup>b</sup>Others are a trace amount of methyl formate mainly.

<sup>c</sup>The hydrocarbons are mainly olefinic C<sub>2</sub> - C<sub>3</sub> hydrocarbons.

**Table 3.** Some catalytic systems with their characteristics for methane activation with soft oxidants such as N<sub>2</sub>O or H<sub>2</sub>O<sub>2</sub>

Catalyst	Oxidant	CH <sub>4</sub> / Oxidant	Rxn condition			Rate of conv. (mmol/(g <sub>cat</sub> ·h))		Product distribution (mol %)					Remarks	Ref.
			P (MPa)	T (°C)	SV (L/(kg <sub>c</sub> at·h))	CH <sub>4</sub>	N <sub>2</sub> O	Oxy.			C <sub>2</sub> =	CO <sub>x</sub>		
								DME	Methanol	HCHO				
V <sub>2</sub> O <sub>5</sub> -SiO <sub>2</sub>	N <sub>2</sub> O	0.5	0.1	480	6575	0.22	-	-	28	44	-	28	with H <sub>2</sub> O	[5]
Mo/Cab-O-Sil	N <sub>2</sub> O	0.27	0.1	560	4788	8.98	-	-	19.9	80.1	-	-	with H <sub>2</sub> O	[6]
				570		13.70	-	-	13.8	64.3	-	21.9	with H <sub>2</sub> O	
20wt% FePO <sub>4</sub> /MCM-41	N <sub>2</sub> O	1	0.1	400	18000	2.25	3.83	25.2	23.6	46.7	-	4.5	-	[7]
				450		6.38	16.34	13.4	20.5	47.5	-	18.6	-	
1.5%Cu/ZSM-5						0.06	0.65	-	89.1	-	-	9.9	-	
1.5%Fe/ZSM-5	H <sub>2</sub> O <sub>2</sub>	13	2	50	430.8	0.03	1.21	-	15.1	-	-	13.6	71.4% of HCOOH	[20]
1.5%Fe- 1.5%Cu/ZSM-5						0.08	1.14	-	92.2	-	-	7.8	-	
FeZSM-5 <sup>a</sup>	N <sub>2</sub> O	10	0.1	275	2500	0.49	0.83	-	2.7	-	2.8	13.3	Coke 81%	[28]
				300		0.80	1.29	-	1.9	-	3.3	18	Coke 76%	
Fe/FeR	N <sub>2</sub> O	2.5	0.1	280	12000	3.11	5.40	27.9	19.6	-	3.5	48.9	-	Present study

<sup>a</sup>The products also contains a trace amount of acetaldehyde.